Milan J. Math. Vol. 80 (2012) 443–467
DOI 10.1007/s00032-012-0194-7
Published online November 7, 2012

Milan Journal of Mathematics

Partitioned Algorithms for Fluid-Structure Interaction Problems in Haemodynamics

Fabio Nobile and Christian Vergara

Abstract. We consider the fluid-structure interaction problem arising in haemodynamic applications. The finite elasticity equations for the vessel are written in Lagrangian form, while the Navier-Stokes equations for the blood in Arbitrary Lagrangian Eulerian form. The resulting three fields problem (fluid/ structure/ fluid domain) is formalized via the introduction of three Lagrange multipliers and consistently discretized by p-th order backward differentiation formulae (BDFp).

We focus on partitioned algorithms for its numerical solution, which consist in the successive solution of the three subproblems. We review several strategies that all rely on the exchange of Robin interface conditions and review their performances reported recently in the literature.

We also analyze the stability of explicit partitioned procedures and convergence of iterative implicit partitioned procedures on a simple linear FSI problem for a general BDFp temporal discretizations.

Mathematics Subject Classification (2010). Primary 65N30; Secondary 76D07.

Keywords. Fluid-structure interaction, incompressible fluids, finite elasticity, haemodynamics, partitioned algorithms, added mass effect.

1. Introduction

The fluid-structure interaction (FSI) problem in large vessels haemodynamics is characterized by a considerable amount of energy exchanged between blood and arterial wall in each cardiac beat [36, 6, 13, 39, 12, 2, 14]. This makes its numerical simulation particularly challenging. Due to the relatively large deformations involved, the structure dynamics is correctly described by non-linear finite elasticity equations. On the other hand, the fluid-dynamics equations to describe blood flow have to be solved in a moving domain. A quite popular approach consists in introducing a so-called *Arbitrary Lagrangian Eulerian* (ALE) formulation [25, 11] that allows to track the moving interface between fluid and solid in a Lagrangian

This work has been partially supported by the ERC Advanced Grant N.227058 MATHCARD and by the Italian MIUR PRIN09 project n. 2009Y4RC3B_001.

way, while keeping the rest of the domain boundary fixed, by introducing a reference configuration and an arbitrary ALE mapping.

The overall FSI problem consists then in three subproblems: the non-linear fluid equations written in ALE formulation in the current moving configuration; the non-linear solid equations written in the reference configuration (Lagrangian formulation); the fluid domain problem to reconstruct the ALE map at each time written in the reference configuration. Such problems are coupled through the *physical interface conditions*, which guarantee the continuity of the velocity and of the normal stresses between fluid and structure, and the *geometrical interface condition*, which guarantees the continuity of displacements between the fluid and the structure domains.

We are here interested in *partitioned algorithms* for the numerical solution of the FSI problem, which consist in the successive solution of the three subproblems [37, 7, 9, 2, 3, 1]. This allows to use separate (pre-existing) solvers for the three subproblems, a feature that is very appealing, since one avoids to construct *ex-novo* a FSI solver and exploits the best solvers available for the ALE-Navier-Stokes and non-linear elasticity equations.

The first aim of this work is to review some recent partitioned algorithms developed in the framework of haemodynamic applications. In particular, we first describe a *naive* approach, based on the successive solution of non-linear fluid and structure problems, until satisfaction of the interface conditions [27, 29, 26]. We then report two schemes based on the application of the quasi-Newton method to the monolithic FSI system. The first one leads to the *Single-Loop* algorithm where both the interface conditions and the constitutive (fluid and structure) non-linearities are treated in the same loop [31, 22, 28, 10, 40, 34]. The second one, introduced in [34], in based on two nested loops, an external one that iterates on the geometrical interface conditions and the constitutive non-linearities, and an internal one that iterates of the physical interface conditions. All these three strategies are presented with Robin interface conditions both for the fluid and for the structure subproblems, leading to the so-called *Robin-Robin* procedures, which generalize the classical *Dirichlet-Neumann* (DN) ones and have been shown to deliver more efficient algorithms [2, 34] with respect to DN approaches. In the case of the double loop algorithm, we review also a strategy to solve the internal linearized FSI problem, by reformulating it as an interface equation [3, 9].

The second aim of this work is to discuss the so called *added mass effect*, which is responsible for the instability of classical explicit DN schemes and for the slow convergence of implicit DN schemes in typical haemodynamic applications. To highlight this phenomenon, we present a stability analysis of the explicit scheme and a convergence analysis of the implicit scheme carried out on a model problem describing the interaction between a potential fluid and a rigid piston with only one degree of freedom. In particular, we extend here the results presented in [7] to a general p-th order temporal discretization of fluid and structure equations, based on *Backward Differentiation Formulae* (BDF).

The outline of the paper is as follows. In Section 2 we describe the fluid and structure subproblems appearing in haemodynamic applications, while in Section 3 we present the coupled problem, its time discretization and a formulation based on Lagrange multipliers. In Section 4 we review the three partitioned algorithms and in Section 4.3 we present the FS interface problem. In Section 5 we discuss the added mass effect and present the stability and convergence analysis. Finally, in Section 6 we discuss and collect recent results on the numerical performances of the presented schemes.

2. Mathematical models for vascular dynamics

2.1. The fluid subproblem in a moving domain

Blood is a concentrated suspension of cellular elements (red blood cells, white blood cells, leukocytes and platelets) in an aqueous polymer solution, the plasma. The latter represents 55% of the blood volume, 92% of which is water with the rest being made up of proteins, small molecules and ions.

While plasma is nearly Newtonian in behavior, whole blood exhibits marked non-Newtonian characteristics at low shear rates due to the deformability of red blood cells and their tendency to form aggregates. In large vessels, however, where shear rate is usually high, the Newtonian rheology is considered acceptable [14] and will be assumed hereafter.

We describe blood dynamics by the Navier-Stokes equations for incompressible, Newtonian fluids, which in Eulerian form read:

$$\begin{cases} \rho_f \dfrac{\partial \boldsymbol{u}_f}{\partial t} + \rho_f(\boldsymbol{u}_f \cdot \nabla)\boldsymbol{u}_f - \nabla \cdot \boldsymbol{T}_f(\boldsymbol{u}_f, p_f) = \boldsymbol{f}_f & \text{in } \Omega_f^t, \\ \nabla \cdot \boldsymbol{u}_f = 0 & \text{in } \Omega_f^t. \end{cases} \tag{2.1}$$

Here $\boldsymbol{u}_f$ and p_f represent the fluid velocity and pressure, respectively, ρ_f is the fluid density, $\boldsymbol{f}_f$ some external forces and $\boldsymbol{T}_f$ is the Cauchy stress tensor, which for Newtonian fluids reads $\boldsymbol{T}_f(\boldsymbol{u}_f, p_f) = \nu(\nabla \boldsymbol{u}_f + \nabla^T \boldsymbol{u}_f) - p_f \boldsymbol{I}$.

Since the domain Ω_f^t changes with time due to the interaction with the arterial wall, from the computational point of view it is convenient to introduce a reference configuration Ω_f^0, typically the diastolic configuration, which can be reconstructed more easily from medical images, and an arbitrary mapping $\mathcal{A}^t : \Omega_f^0 \to \Omega_f^t$, called *Arbitrary Lagrangian Eulerian* map. In particular, referring to Figure 1, the inflow and outflow sections $\Sigma_{f,i}^t$ will remain unchanged by the mapping, while the reference interface Σ^0 will be tracked in a Lagrangian way and mapped into the deformed interface Σ^t. For any function g_f defined in the current domain Ω_f^t, we denote by $\tilde{g}_f = g_f \circ \mathcal{A}^t$ its counterpart in the reference domain Ω_f^0. We also introduce the domain velocity $\widetilde{\boldsymbol{u}}_m = \frac{\partial \mathcal{A}^t}{\partial t}$ and its counterpart $\boldsymbol{u}_m = \widetilde{\boldsymbol{u}}_m \circ (\mathcal{A}^t)^{-1}$. Then, the Navier-Stokes

equations written in ALE form in the current configuration read:

$$\begin{cases} \rho_f \dfrac{D^A \boldsymbol{u}_f}{Dt} + \rho_f((\boldsymbol{u}_f - \boldsymbol{u}_m)\cdot\nabla)\boldsymbol{u}_f - \nabla\cdot\boldsymbol{T}_f(\boldsymbol{u}_f, p_f) = \boldsymbol{f}_f & \text{in } \Omega_f^t, \\ \nabla\cdot\boldsymbol{u}_f = 0 & \text{in } \Omega_f^t, \end{cases} \tag{2.2}$$

where we have used the ALE time derivative $\frac{D^A \boldsymbol{u}_f}{Dt} = \frac{\partial \widetilde{\boldsymbol{u}}_f}{\partial t} \circ (\mathcal{A}^t)^{-1}$. Several strategies can be adopted to practically compute the ALE map for a given displacement of the moving interface Σ^t. In what follows, we consider a simple procedure based on the computation of a harmonic extension of the boundary displacement inside the fluid domain. Although this procedure does not guarantee the map to be invertible, numerical evidence shows that it is robust enough for the applications at hand.

2.2. The structure subproblem

Arterial walls are made of three circumferential layers: intima, media and adventitia. From the mechanical perspective, the media is the most significant layer in healthy arteries and is made primarily by elastin and collagen fibers. The elastic tissue can make up more than 50% of the dry weight of the large arteries. The collagen fibres are oriented in a roughly helical form around the artery and are generally tortuous under normal conditions. As the artery is distended, the collagen fibres straighten and, because of their large tensile strength, bear more and more of the load.

Since the deformation of large arteries during a cardiac beat is quite large, the correct framework to describe its dynamics is given by the finite elasticity equations. Let Ω_s^0 be the reference configuration for the arterial wall. We describe the arterial motion by the displacement field $\widetilde{\boldsymbol{\eta}}_s = \widetilde{\boldsymbol{\eta}}_s(\boldsymbol{x}_s^0, t)$ of each material $\boldsymbol{x}_s^0 \in \Omega_s^0$ in time. The deformed configuration is denoted by Ω_s^t and the current position on each material point is individuated by the Lagrangian map $\boldsymbol{x}_s^t = \mathcal{L}^t(\boldsymbol{x}_s^0) = \boldsymbol{x}_s^0 + \widetilde{\boldsymbol{\eta}}_s^0(\boldsymbol{x}_s^0, t)$. For each function $f : \Omega_s^t \to \mathbb{R}$ defined on the current configuration we denote by $\widetilde{f} = f \circ \mathcal{L}^t$ its counterpart in the reference configuration.

The deformation of the tissue is measured in terms of the deformation gradient tensor $\boldsymbol{F} = \boldsymbol{I} + \nabla\widetilde{\boldsymbol{\eta}}_s$ and the right Cauchy-Green tensor $\boldsymbol{C} = \boldsymbol{F}^T\boldsymbol{F}$. The Cauchy stress tensor is denoted by $\boldsymbol{T}_s$ in the current configuration whereas the corresponding stress tensor in the reference configuration (first Piola-Kirchhoff tensor) is denoted by $\widetilde{\boldsymbol{T}}_s = J\boldsymbol{T}_s\boldsymbol{F}^{-T}$, with $J = \det(\boldsymbol{F})$.

Then, the dynamics of the arterial tissue is governed, in Lagrangian form, by the equation

$$\rho_s \frac{\partial^2 \widetilde{\boldsymbol{\eta}}_s}{\partial t^2} - \nabla\cdot\widetilde{\boldsymbol{T}}_s(\widetilde{\boldsymbol{\eta}}_s) = \widetilde{\boldsymbol{f}}_s \quad \text{in } \Omega_s^0, \ \ t > 0,$$

where ρ_s is the tissue density and $\widetilde{\boldsymbol{f}}_s$ external forces acting on the system.

Soft biological tissues can be regarded as elastic under relatively large deformations, so it is common to derive the Cauchy stress tensor from a strain energy function $\mathcal{W} = \mathcal{W}(\boldsymbol{C})$, i.e. $\widetilde{\boldsymbol{T}}_s = 2\boldsymbol{F}\frac{\partial \mathcal{W}}{\partial \boldsymbol{C}}$. Several models have been proposed for the strain energy function. We point to [24] for a recent review. We consider here nearly incompressible models where the strain energy function is decomposed into

an isochoric and a volumetric part

$$\mathcal{W} = \mathcal{W}_{iso}(\bar{\boldsymbol{C}}) + \mathcal{W}_{vol}(J), \quad \text{with } \bar{\boldsymbol{C}} = J^{-\frac{2}{3}}\boldsymbol{C}.$$

The volumetric part penalizes the changes of volume. A possible expression is given by $\mathcal{W}_{vol} = \frac{\kappa}{4}[(J-1)^2 + (\log J)^2]$. For the isochoric strain energy function, a widely used model is the exponential one [17, 23, 42]

$$\mathcal{W}_{iso} = \frac{\alpha}{2\gamma}\left(\exp\{\gamma(\mathrm{tr}(\bar{\boldsymbol{C}}) - 3)\} - 1\right)$$

which describes the strong stiffening effect of the tissue observed at higher loadings due to collagen fibres. More sophisticated models [24] take into account the preferential direction of the collagen fibers, characterized by a unit vector field $\boldsymbol{M}$ in the reference configuration. They combine a neo-Hookean model to describe elastin behavior, with an exponential model along the preferential direction (or multiple directions) of the collagen fibers. For a single direction the strain energy function proposed in [23] reads:

$$\mathcal{W}_{iso} = \frac{\mu}{2}(\mathrm{tr}(\bar{\boldsymbol{C}}) - 3) + \frac{\alpha}{2\gamma}\left(\exp\{\gamma(\boldsymbol{M}^T\bar{\boldsymbol{C}}\boldsymbol{M} - 1)^2\} - 1\right).$$

We point out, however, that in patient specific simulations and geometries reconstructed from medical images, it is very difficult to date to extract the information on the fibers direction.

3. The coupled fluid-structure interaction problem

3.1. Continuous formulation

We consider a coupled system obtained by the interaction between a fluid and a structure, whose separate description has been given in the previous section. Again, Ω_f^t and Ω_s^t represent the current fluid and structure domains, respectively, while Σ^t indicates the fluid-structure interface, see Figure 1. The same quantities with superscript ^{0} refer instead to the reference configuration and functions defined therein are denoted with a tilde. Moreover, by $\boldsymbol{n}_f$ (resp. $\boldsymbol{n}_s$) we denote the unit outward normal vector to $\partial\Omega_f^t$ (resp. $\partial\Omega_s^t$). The strong formulation of the FSI problem, including the computation of the ALE map reads then as follows

1. *Fluid-Structure problem.* Given the (unknown) fluid domain velocity $\boldsymbol{u}_m$ and fluid domain Ω_f^t, find, at each time $t \in (0, T]$, the fluid velocity $\boldsymbol{u}_f$, pressure p_f

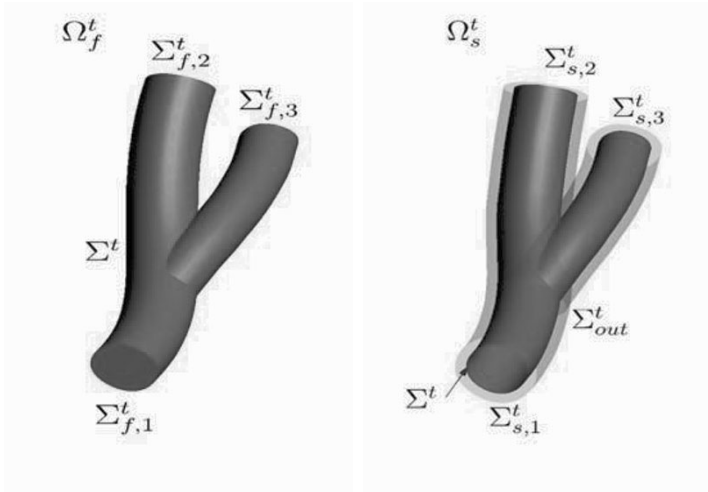

FIGURE 1. Representation of the domain of the FSI problem: fluid domain on the left, structure domain on the right.

and structure displacement $\boldsymbol{\eta}_s$ such that

$$\begin{cases} \rho_f \dfrac{D^A \boldsymbol{u}_f}{Dt} + \rho_f((\boldsymbol{u}_f - \boldsymbol{u}_m)\cdot\nabla)\boldsymbol{u}_f - \nabla\cdot\boldsymbol{T}_f(\boldsymbol{u}_f, p_f) = \boldsymbol{f}_f & \text{in } \Omega_f^t, \\ \nabla\cdot\boldsymbol{u}_f = 0 & \text{in } \Omega_f^t, \\ \rho_s \dfrac{\partial^2 \widetilde{\boldsymbol{\eta}}_s}{\partial t^2} - \nabla\cdot\widetilde{\boldsymbol{T}}_s(\widetilde{\boldsymbol{\eta}}_s) = \widetilde{\boldsymbol{f}}_s & \text{in } \Omega_s^0, \\ \boldsymbol{u}_f = \dfrac{\partial \boldsymbol{\eta}_s}{\partial t} & \text{on } \Sigma^t, \\ \boldsymbol{T}_s(\boldsymbol{\eta}_s)\,\boldsymbol{n}_s + \boldsymbol{T}_f(\boldsymbol{u}_f, p_f)\,\boldsymbol{n}_f = \boldsymbol{0} & \text{on } \Sigma^t, \\ \alpha_e \widetilde{\boldsymbol{\eta}}_s + \widetilde{\boldsymbol{T}}_s(\widetilde{\boldsymbol{\eta}}_s)\,\widetilde{\boldsymbol{n}}_s = P_{ext}\widetilde{\boldsymbol{n}}, & \text{on } \Sigma_{out}^0. \end{cases} \tag{3.1}$$

2. *Geometry problem.* Given the (unknown) interface structure displacement $\widetilde{\boldsymbol{\eta}}_s|_{\Sigma^0}$, find the displacement of the points of the fluid domain $\boldsymbol{\eta}_m$ such that

$$\begin{cases} -\triangle\widetilde{\boldsymbol{\eta}}_m = \boldsymbol{0} \quad \text{on } \Omega_f^0, \\ \widetilde{\boldsymbol{\eta}}_m = \widetilde{\boldsymbol{\eta}}_s \quad \text{on } \Sigma^0, \end{cases} \tag{3.2}$$

and then find accordingly the fluid domain velocity $\widetilde{\boldsymbol{u}}_m := \frac{\partial \widetilde{\boldsymbol{\eta}}_m}{\partial t}$, and the new points $\boldsymbol{x}_f^t$ of the fluid domain by moving the points $\boldsymbol{x}_f^0$ of the reference domain Ω_f^0: $\boldsymbol{x}_f^t = \boldsymbol{x}_f^0 + \widetilde{\boldsymbol{\eta}}_m$.

The two matching conditions enforced at the FS interface are the *continuity of velocities* $(3.1)_4$ and the *continuity of normal stresses* $(3.1)_5$ (physical interface conditions), while condition $(3.2)_2$ enforces that the fluid domain remains at all time in contact with the solid (geometrical interface condition). Equations (3.1) and (3.2) have to be endowed with suitable boundary conditions on $\Omega_f^t \setminus \Sigma^t$ and $\Omega_s^0 \setminus (\Sigma^0 \cup \Sigma_{out}^0)$, and with suitable initial conditions. The Robin boundary condition $(3.1)_6$

on Σ^0_{out} models the presence of a surrounding tissue around the vessel. This choice corresponds to model the tissue as a perfectly elastic body, with α_e the corresponding elastic coefficient (see [33, 30]).

3.2. Temporal discretization

For the temporal discretization we consider here BDF schemes (see e.g. [20]) applied to both the fluid and the structure subproblems. In particular, let Δt be the time discretization parameter and $t^n := n\,\Delta t$, $n = 0, 1, \ldots$. For a generic function z, we denote with z^n the approximation of $z(t^n)$. We consider general discretizations of order p (BDFp) of the form

$$\begin{aligned} \frac{D_p v^{n+1}}{\Delta t} &:= \frac{1}{\Delta t}\left(\beta_0\, v^{n+1} - \sum_{i=1}^{p} \beta_i\, v^{n+1-i}\right) = \frac{\partial v}{\partial t}(t^{n+1}) + O(\Delta t^p), \\ \frac{D_p^2 v^{n+1}}{\Delta t^2} &:= \frac{1}{\Delta t^2}\left(\xi_0\, v^{n+1} - \sum_{i=1}^{p+1} \xi_i\, v^{n+1-i}\right) = \frac{\partial^2 v}{\partial t^2}(t^{n+1}) + O(\Delta t^p), \end{aligned} \tag{3.3}$$

for suitable coefficients β_i and ξ_i. In Table 1 we report the values of such parameters for $p = 1, 2, 3, 4$.

	β_0	β_1	β_2	β_3	β_4	ξ_0	ξ_1	ξ_2	ξ_3	ξ_4	ξ_5
1	1	1	–	–	–	1	2	-1	–	–	–
2	3/2	2	-1/2	–	–	2	5	-4	1	–	–
3	11/6	3	-3/2	1/3	–	35/12	26/3	-19/2	14/3	-11/12	–
4	25/12	4	-3	4/3	-1/4	15/4	77/6	-107/6	13	-61/12	5/6

TABLE 1. Values of parameters β_i and ξ_i for BDFp schemes involved in the discretization of first (left) and second (right) derivatives - $p = 1, 2, 3, 4$.

For the sake of notation in what follows we will omit the index of the current time step $^{n+1}$. Then, the discretized-in-time FSI problems at time t^{n+1} is obtained by (3.1) – (3.2) where the time derivative operators are replaced by approximations (3.3).

3.3. A three field formulation by Lagrange multipliers

The FSI monolithic system (3.1) – (3.2) and its discretized-in-time version consist of three partial differential equations coupled through three interface conditions: the fluid and the structure subproblems share the same velocity and the same normal stress (physical conditions), while the fluid domain and the structure domain share the same displacement (geometrical condition).

In order to highlight the coupled structure of the problem, we report here an equivalent formulation introduced in [34] based on the introduction of three Lagrange multipliers defined on the FS interface, representing the fluid and structure

normal stresses $\boldsymbol{\lambda}_f = -\boldsymbol{T}_f \boldsymbol{n}_f$ and $\boldsymbol{\lambda}_s = -\boldsymbol{T}_s \boldsymbol{n}_s$, and the normal derivative of the fluid mesh displacement $\boldsymbol{\lambda}_m = -\nabla \boldsymbol{\eta}_m \cdot \boldsymbol{n}_f$. This will be useful also for the derivation of partitioned algorithms for the numerical solution of the coupled problem. In particular, with Σ_f^D, $\Sigma_s^{D,0}$ and Σ_m^D we denote the parts of the boundary where Dirichlet boundary conditions are prescribed. To lighten the notation, we drop hereafter the superscript $n+1$ also for domains and spaces, so that, if not otherwise specified, they have to be intended at time t^{n+1}. Then, we define the following functional spaces

$$V_f := \{v \in H^1(\Omega_f) : \, v|_{\Sigma_f^D} = 0\}, \qquad Q := L^2(\Omega_f),$$

$$V_s := \{v \in H^1(\Omega_s^0) : \, v|_{\Sigma_s^{D,0}} = 0\}, \qquad V_m := \{v \in H^1(\Omega_f^0) : \, v|_{\Sigma_m^{D,0}} = 0\},$$

where the conditions imposed on the boundaries have to be intended in the sense of traces. Let $\boldsymbol{v}_f := (\boldsymbol{u}_f, p_f)$ collect the fluid unknowns and $\mathcal{F} : \boldsymbol{V}_f \times Q \times \boldsymbol{V}_m \to (\boldsymbol{V}_f \times Q)'$ be the discretized-in-time fluid operator. Analogously, for the structure subproblem we define the discretized-in-time operator $\mathcal{S} : \boldsymbol{V}_s \to (\boldsymbol{V}_s)'$, and for the harmonic extension we introduce the operator $\mathcal{H} : \boldsymbol{V}_m \to (\boldsymbol{V}_m)'$. We also define the following trace operators

$$\begin{aligned}
&\widetilde{\gamma}_f : \boldsymbol{V}_f \times Q \to \boldsymbol{H}^{1/2}(\Sigma^0), \ \widetilde{\gamma}_f(\boldsymbol{v}, q) := \widetilde{\boldsymbol{v}}|_{\Sigma^0}\,, \\
&\gamma_f : \boldsymbol{V}_f \times Q \to \boldsymbol{H}^{1/2}(\Sigma), \ \gamma_f(\boldsymbol{v}, q) := \boldsymbol{v}|_{\Sigma}\,, \\
&\widetilde{\gamma}_s : \boldsymbol{V}_s \to \boldsymbol{H}^{1/2}(\Sigma^0), \ \widetilde{\gamma}_s \widetilde{\boldsymbol{\mu}} := \widetilde{\boldsymbol{\mu}}|_{\Sigma^0}\,, \\
&\gamma_s : \boldsymbol{V}_s \to \boldsymbol{H}^{1/2}(\Sigma), \ \gamma_s \widetilde{\boldsymbol{\mu}} := \boldsymbol{\mu}|_{\Sigma}\,, \\
&\widetilde{\gamma}_m : \boldsymbol{V}_m \to \boldsymbol{H}^{1/2}(\Sigma^0), \ \widetilde{\gamma}_m \widetilde{\boldsymbol{z}} := \widetilde{\boldsymbol{z}}|_{\Sigma^0}\,.
\end{aligned}$$

We then rewrite the time discrete version of problem (3.1)-(3.2) as follows

$$\left\{\begin{array}{rcll}
\mathcal{H}\,\widetilde{\boldsymbol{\eta}}_m + \widetilde{\gamma}_m^* \widetilde{\boldsymbol{\lambda}}_m &=& \boldsymbol{0} & \text{in } (\boldsymbol{V}_m)', \\
\widetilde{\gamma}_m \widetilde{\boldsymbol{\eta}}_m &=& \widetilde{\gamma}_s \widetilde{\boldsymbol{\eta}}_s & \text{on } \Sigma^0, \\
\mathcal{F}(\boldsymbol{v}_f, \boldsymbol{u}_m) + \gamma_f^* \boldsymbol{\lambda}_f &=& \mathcal{G}_f & \text{in } (\boldsymbol{V}_f \times Q)', \\
\widetilde{\gamma}_f \boldsymbol{v}_f &=& \widetilde{\gamma}_s \frac{D_p \widetilde{\boldsymbol{\eta}}_s}{\Delta t} & \text{on } \Sigma^0, \\
\widetilde{\boldsymbol{\lambda}}_s &=& -\widetilde{\boldsymbol{\lambda}}_f & \text{on } \Sigma^0, \\
\mathcal{S}(\widetilde{\boldsymbol{\eta}}_s) + \widetilde{\gamma}_s^* \widetilde{\boldsymbol{\lambda}}_s &=& \mathcal{G}_s & \text{in } (\boldsymbol{V}_s)',
\end{array}\right. \tag{3.4}$$

where $\boldsymbol{u}_m = \frac{D_p \boldsymbol{\eta}_m}{\Delta t}$ and where γ^* denotes the adjoint of the trace operator, $\mathcal{G}_s$ and $\mathcal{G}_f$ accounting for the right-hand sides. See [34] for more details.

4. Partitioned algorithms based on Robin interface conditions

Among the strategies which could be considered for the numerical solution of the FSI problem, a particular attention has been devoted to partitioned algorithms. These strategies are based on the successive solution of the three subproblems and allows one to reuse existing codes. They could be *explicit* (staggered), in which case the fluid and structure subproblems are solved only once (or few times) for time steps, or *implicit*, in which case the subproblems are solved iteratively until the interface

conditions are satisfied [37, 7, 9, 12, 5, 2]. Recently, also *semi-implicit* algorithms have been proposed, in which the ALE-geometry problem is solved only once per time step, whereas the fluid and structure problems are iterated [12, 5, 34]. In this case, the interface physical conditions $(3.4)_{4-5}$ are enforced exactly at each time step, whereas the interface geometrical condition $(3.4)_2$ is enforced only in an approximate way.

In haemodynamics, the use of explicit partitioned algorithms turns out to be extremely problematic for stability reasons, because of the large added-mass of the fluid on the structure. This issue is discussed thoroughly in Section 5 (see also [7, 16]). Implicit partitioned algorithms are also affected by the added mass effect as they feature very slow convergence, unless special treatments of the interface conditions are considered. We focus here on procedures in which the fluid and structure subproblems are solved enforcing Robin interface conditions [2, 3, 1, 8, 43]. The use of Robin-Robin interface conditions can significantly alleviate the added mass effect if the coefficients in the Robin conditions are properly chosen, as shown in [2, 19].

To derive such algorithms in a general framework, we consider system (3.4) where the two physical interface conditions $(3.4)_{4-5}$ are replaced by linear combinations of them:

$$\left\{\begin{array}{rcll} \alpha_f\,\widetilde{\gamma}_f\boldsymbol{v}_f + \widetilde{\boldsymbol{\lambda}}_f &=& \alpha_f\widetilde{\gamma}_s\frac{D_p\widetilde{\boldsymbol{\eta}}_s}{\Delta t} - \widetilde{\boldsymbol{\lambda}}_s & \text{on } \Sigma^0, \\ \alpha_s\widetilde{\gamma}_s\dfrac{D_p\widetilde{\boldsymbol{\eta}}_s}{\Delta t} + \widetilde{\boldsymbol{\lambda}}_s &=& \alpha_s\widetilde{\gamma}_f\boldsymbol{v}_f - \widetilde{\boldsymbol{\lambda}}_f & \text{on } \Sigma^0. \end{array}\right. \tag{4.1}$$

If $\alpha_f \neq \alpha_s$ then these new physical interface conditions are equivalent to $(3.4)_{4-5}$. In the following sections, we present some Robin-Robin formulations adapted to the case of the finite elasticity. In any case, the Lagrange multipliers have been introduced just to simplify the expression of the three interface continuity conditions and the derivation of the partitioned algorithms. However, there is no actual need to introduce them in practical implementations of the algorithms to avoid extra costs. We also observe that the classical Dirichlet-Neumann (DN) formulations are recovered from the Robin-Robin ones by setting $\alpha_f \to \infty$ and $\alpha_s = 0$.

4.1. Robin-Robin standard iterations

The first strategy corresponds to simple iterations at each time step between the fluid and the structure subproblems with Robin boundary conditions (see [27, 29, 26] for the DN case). It corresponds to a block-Gauss-Seidel method applied to system (3.4) where conditions $(3.4)_{4-5}$ are replaced by (4.1). We have the following

Algorithm 1.

Given the solution at iteration k, solve until convergence

1. The (non-linear) fluid problem in ALE configuration with Robin interface condition and the geometry problem

$$\begin{cases} \mathcal{H}\,\widetilde{\boldsymbol{\eta}}_m^{k+1} + \widetilde{\gamma}_m^*\widetilde{\boldsymbol{\lambda}}_m^{k+1} &= \mathbf{0} & \text{in } (\boldsymbol{V}_m)', \\ \widetilde{\gamma}_m\widetilde{\boldsymbol{\eta}}_m^{k+1} &= \widetilde{\gamma}_s\widetilde{\boldsymbol{\eta}}_s^{k} & \text{on } \Sigma^0, \\ \mathcal{F}(\boldsymbol{v}_f^{k+1}, \boldsymbol{u}_m^{k+1}) + \widetilde{\gamma}_f^*\widetilde{\boldsymbol{\lambda}}_f^{k+1} &= \mathcal{G}_f & \text{in } \left(\boldsymbol{V}_f(\boldsymbol{\eta}_s^k)\times Q(\boldsymbol{\eta}_s^k)\right)', \\ \alpha_f\,\gamma_f\boldsymbol{v}_f^{k+1} + \boldsymbol{\lambda}_f^{k+1} &= \alpha_f\gamma_s\tfrac{D_p\boldsymbol{\eta}_s^k}{\Delta t} - \boldsymbol{\lambda}_s^k & \text{on } \Sigma^{k+1}; \end{cases} \tag{4.2}$$

2. The (non-linear) structure problem with Robin interface condition

$$\begin{cases} \mathcal{S}(\widetilde{\boldsymbol{\eta}}_s^{k+1}) + \widetilde{\gamma}_s^*\widetilde{\boldsymbol{\lambda}}_s^{k+1} &= \mathcal{G}_s & \text{in } (\boldsymbol{V}_s)', \\ \alpha_s\,\widetilde{\gamma}_s\tfrac{D_p\widetilde{\boldsymbol{\eta}}_s^{k+1}}{\Delta t} + \widetilde{\boldsymbol{\lambda}}_s^{k+1} &= \alpha_s\widetilde{\gamma}_f\boldsymbol{v}_f^{k+1} - \widetilde{\boldsymbol{\lambda}}_f^{k+1} & \text{on } \Sigma^0. \end{cases}$$

We monitor the residuals of equations $(4.2)_2$ and $(4.2)_4$ and stop the iterations when such residuals are below a prescribed tolerance. In problem (4.2), we have denoted by $\boldsymbol{V}_f(\boldsymbol{\xi})$ and $Q(\boldsymbol{\xi})$ the spaces defined on the domain Ω_f obtained by the harmonic extension of the datum $\boldsymbol{\xi}$. We also observe that the solution of the geometry problem does not depend on the fluid solution, therefore at each Robin-Robin iteration the harmonic extension could be solved separately. Then, Algorithm 1 consists in the successive solution of a harmonic extension, a non-linear fluid problem in a known domain and a non-linear structure problem. The last two subproblems have to be solved with a proper strategy to handle the non-linearities, such as with Picard iterations for the fluid and Newton iterations for the structure.

Algorithm 1 is particularly suited when one has at disposal two *black-box* solvers for the fluid problem in ALE formulation and for the structure, since it needs just to implement suitable routines for the transfer of the interface conditions between the two codes.

4.2. Quasi-Newton methods

We rewrite system (3.4) where conditions $(3.4)_{4-5}$ are replaced by (4.1) in a compact form as $\boldsymbol{G}(\boldsymbol{y}) = \mathbf{0}$, where $\boldsymbol{y} := [\widetilde{\boldsymbol{\eta}}_m, \widetilde{\boldsymbol{\lambda}}_m, \boldsymbol{v}_f, \widetilde{\boldsymbol{\lambda}}_f, \widetilde{\boldsymbol{\lambda}}_s, \widetilde{\boldsymbol{\eta}}_s]$ denotes the FSI solution. A second strategy to solve the FSI problem with partitioned algorithms consists in writing quasi-Newton iterations applied to $\boldsymbol{G}(\boldsymbol{y}) = \mathbf{0}$, that is

$$\widehat{J}(\boldsymbol{y}^k)\,\delta\boldsymbol{y}^{k+1} = -\boldsymbol{G}(\boldsymbol{y}^k), \tag{4.3}$$

where $\widehat{J}$ is a suitable approximation of the Jacobian [21, 31, 28, 34]

$$\nabla\boldsymbol{G} = \left[\begin{array}{cc|cc|cc} \mathcal{H} & \widetilde{\gamma}_m^* & & & & -\widetilde{\gamma}_s \\ \widetilde{\gamma}_m & & & & & \\ \hline \nabla_{\eta_m}\mathcal{F} & & \nabla_{v_f}\mathcal{F} & \widetilde{\gamma}_f^* & & \\ & & \alpha_f\widetilde{\gamma}_f & I & I & -\alpha_f\frac{\beta_0\widetilde{\gamma}_s}{\Delta t} \\ \hline & & -\alpha_s\widetilde{\gamma}_f & I & I & \alpha_s\frac{\beta_0\gamma_s}{\Delta t} \\ & & & & \widetilde{\gamma}_s^* & \nabla_{\eta_s}\mathcal{S} \end{array}\right].$$

The partitioned algorithms we investigate in this work are all derived by (4.3) by a proper choice of $\widehat{J}$. In all cases, the approximation of the Jacobian is chosen such that

1. The term $\nabla_{\eta_m}\mathcal{F}$ representing the shape derivative is neglected;

2. The tangent fluid problem $\nabla_{v_f}\mathcal{F}$ is replaced by an Oseen problem

$$\widehat{\nabla}_{v_f}\mathcal{F}\,\delta\boldsymbol{v}_f := \begin{cases} \rho_f\dfrac{\beta_0}{\Delta t}\delta\boldsymbol{u}_f + \rho_f((\boldsymbol{u}_f-\boldsymbol{u}_m)\cdot\nabla)\delta\boldsymbol{u}_f - \nabla\cdot\boldsymbol{T}_f(\delta\boldsymbol{u}_f,\delta p_f) \\ \nabla\cdot\delta\boldsymbol{u}_f, \end{cases}$$

with a known convective term extrapolated from previous time steps. In order to make clearer its expression, we will indicate explicitly the convective term in the Oseen operator as $\widehat{\nabla}_{v_f}\mathcal{F}(\boldsymbol{w})$.

The residual $\widehat{J}(\boldsymbol{y}^k)\,\delta\boldsymbol{y}^{k+1} + \boldsymbol{G}(\boldsymbol{y}^{k+1})$ is used to monitor the convergence of the iterations, leading case by case to different stopping criteria [34].

4.2.1. Single-loop algorithm. We consider a three blocks diagonal approximation of the Jacobian [31, 22, 28, 10, 40, 34], that is

$$\widehat{J}_{SL} = \left[\begin{array}{cc|cc|cc} \mathcal{H} & \widetilde{\gamma}_m^* & & & & \\ \widetilde{\gamma}_m & & & & & \\ \hline & & \widehat{\nabla}_{v_f}\mathcal{F} & \widetilde{\gamma}_f^* & & \\ & & \alpha_f\widetilde{\gamma}_f & I & & \\ \hline & & -\alpha_s\widetilde{\gamma}_f & I & I & \alpha_s\frac{\beta_0\widetilde{\gamma}_s}{\Delta t} \\ & & & & \widetilde{\gamma}_s^* & \nabla_{\eta_s}\mathcal{S} \end{array}\right],$$

which leads to the following

Algorithm 2.

Given the solution at iteration k, solve until convergence

1. The harmonic extension

$$\begin{cases} \mathcal{H}\,\widetilde{\boldsymbol{\eta}}_m^{k+1} + \widetilde{\gamma}_m^*\widetilde{\boldsymbol{\lambda}}_m^{k+1} = 0 & \text{in } (\boldsymbol{V}_m)', \\ \widetilde{\gamma}_m\widetilde{\boldsymbol{\eta}}_m^{k+1} = \widetilde{\gamma}_s\widetilde{\boldsymbol{\eta}}_s^{k} & \text{on } \Sigma^0, \end{cases}$$

obtaining the new fluid domain Ω_f^{k+1} and the domain velocity $\boldsymbol{u}_m^{k+1}$.

2. The fluid subproblem with a Robin condition at the FS interface

$$\begin{cases} \widehat{\nabla}_{v_f}\mathcal{F}(\boldsymbol{u}_f^k - \boldsymbol{u}_m^{k+1})\,\boldsymbol{v}_f^{k+1} + \widetilde{\gamma}_f^*\widetilde{\boldsymbol{\lambda}}_f^{k+1} = \mathcal{G}_f & \text{in } \left(\boldsymbol{V}_f(\boldsymbol{\eta}_s^k)\times Q(\boldsymbol{\eta}_s^k)\right)', \\ \alpha_f\gamma_f\boldsymbol{v}_f^{k+1} + \boldsymbol{\lambda}_f^{k+1} = \alpha_f\gamma_s\frac{D_p\boldsymbol{\eta}_s^k}{\Delta t} - \boldsymbol{\lambda}_s^k & \text{on } \Sigma^{k+1}, \end{cases} \tag{4.4}$$

3. The structure subproblem with a Robin condition at the FS interface

$$\begin{cases} \nabla_{\eta_s}\mathcal{S}(\widetilde{\boldsymbol{\eta}}_s^k)\,\delta\widetilde{\boldsymbol{\eta}}_s^{k+1} + \widetilde{\gamma}_s^*\delta\widetilde{\boldsymbol{\lambda}}_s^{k+1} = \mathcal{G}_s - \mathcal{S}(\widetilde{\boldsymbol{\eta}}_s^k) - \widetilde{\gamma}_s^*\widetilde{\boldsymbol{\lambda}}_s^k & \text{in } (\boldsymbol{V}_s)', \\ \alpha_s\widetilde{\gamma}_s\frac{D_p\widetilde{\boldsymbol{\eta}}_s^{k+1}}{\Delta t} - \widetilde{\boldsymbol{\lambda}}_s^{k+1} = \alpha_s\widetilde{\gamma}_f\,\widetilde{\boldsymbol{v}}_f^{k+1} - \widetilde{\boldsymbol{\lambda}}_f^{k+1} & \text{on } \Sigma^0. \end{cases}$$

We observe that with this choice we obtain again a partitioned algorithm corresponding to the sequential solution of the harmonic extension, fluid subproblem and structure subproblem. However, in this case, differently from Algorithm 1, the fluid and the structure subproblems are linear at each iteration. Indeed, in this case, the geometrical and physical interface conditions and the constitutive non-linearities are all treated in the same loop.

This algorithm can be implemented in a modular way provided one has access to an Oseen-ALE solver and to a tangent structure solver, both with the possibility of prescribing Robin boundary conditions.

4.2.2. Double-loop algorithm. We consider here a two blocks diagonal approximation of the Jacobian [34], that is

$$\widehat{J}_{DL} = \left[\begin{array}{cc|cc|cc} \mathcal{H} & \widetilde{\gamma}_m^* & & & & \\ \widetilde{\gamma}_m & & & & & \\ \hline & & \widehat{\nabla}_{v_f}\mathcal{F} & \widetilde{\gamma}_f^* & & \\ & & \alpha_f\widetilde{\gamma}_f & I & I & -\alpha_f\frac{\beta_0\widetilde{\gamma}_s}{\Delta t} \\ \hline & & -\alpha_s\widetilde{\gamma}_f & I & I & \alpha_s\frac{\beta_0\widetilde{\gamma}_s}{\Delta t} \\ & & & & \widetilde{\gamma}_s^* & \nabla_{\eta_s}\mathcal{S} \end{array}\right],$$

which corresponds to the sequential solution of the harmonic extension and of a linearized FSI problem. For the solution of the latter, since we are interested in partitioned algorithms, we use the following RR preconditioner

$$\widehat{P}_{RR} = \left[\begin{array}{cc|cc} \widehat{\nabla}_{v_f}\mathcal{F} & \widetilde{\gamma}_f^* & & \\ \alpha_f\widetilde{\gamma}_f & I & & \\ \hline -\alpha_s\widetilde{\gamma}_f & I & I & \alpha_s\frac{\beta_0}{\Delta t}\widetilde{\gamma}_s \\ & & \widetilde{\gamma}_s^* & \nabla_{\eta_s}\mathcal{S} \end{array}\right].$$

We obtain the following:

Algorithm 3.

Given the solution at iteration k, solve until convergence

1. The harmonic extension

$$\left\{\begin{array}{ll} \mathcal{H}\,\widetilde{\boldsymbol{\eta}}_m^{k+1} + \widetilde{\gamma}_m^*\widetilde{\boldsymbol{\lambda}}_m^{k+1} = 0 & \text{in } (\boldsymbol{V}_m)', \\ \widetilde{\gamma}_m\widetilde{\boldsymbol{\eta}}_m^{k+1} = \widetilde{\gamma}_s\widetilde{\boldsymbol{\eta}}_s^{k} & \text{on } \Sigma^0, \end{array}\right.$$

   obtaining the new fluid domain and fluid domain velocity.
2. The linearized FSI problem. For its solution, we consider the following partitioned algorithm: Given the solution at subiteration $l-1$, solve at the current subiteration l until convergence
   (a) The fluid subproblem with Robin condition at the FS interface

$$\left\{\begin{array}{ll} \widehat{\nabla}_{v_f}\mathcal{F}(\boldsymbol{u}_{f,l}^k - \boldsymbol{u}_m^{k+1})\,\boldsymbol{v}_{f,l}^{k+1} + \widetilde{\gamma}_f^*\widetilde{\boldsymbol{\lambda}}_{f,l}^{k+1} = \mathcal{G}_f & \text{in } \left(\boldsymbol{V}_f(\boldsymbol{\eta}_s^k)\times Q(\boldsymbol{\eta}_s^k)\right)', \\ \alpha_f\gamma_f\boldsymbol{v}_{f,l}^{k+1} + \boldsymbol{\lambda}_{f,l}^{k+1} = \alpha_f\gamma_s\frac{D_p\boldsymbol{\eta}_{s,l-1}^k}{\Delta t} - \boldsymbol{\lambda}_{s,l-1}^k & \text{on } \Sigma^{k+1}, \end{array}\right.$$

   (b) The structure subproblem with Robin condition at the FS interface

$$\left\{\begin{array}{ll} \nabla_\eta\mathcal{S}(\widetilde{\boldsymbol{\eta}}_{s,l}^k)\,\delta\widetilde{\boldsymbol{\eta}}_{s,l}^{k+1} + \widetilde{\gamma}_s^*\delta\widetilde{\boldsymbol{\lambda}}_{s,l}^{k+1} = \mathcal{G}_s - \mathcal{S}(\widetilde{\boldsymbol{\eta}}_s^k) - \widetilde{\gamma}_s^*\widetilde{\boldsymbol{\lambda}}_s^k & \text{in } (\boldsymbol{V}_s)', \\ \alpha_s\widetilde{\gamma}_s\frac{D_p\widetilde{\boldsymbol{\eta}}_{s,l}^{k+1}}{\Delta t} - \widetilde{\boldsymbol{\lambda}}_{s,l}^{k+1} = \alpha_s\widetilde{\gamma}_f\,\widetilde{\boldsymbol{v}}_{f,l}^{k+1} - \widetilde{\boldsymbol{\lambda}}_{f,l}^{k+1} & \text{on } \Sigma^0. \end{array}\right.$$

This algorithm contains two nested loops, an external one for the prescription of the geometrical continuity condition and for the treatment of the constitutive non-linearities, and an internal one for the prescription of the physical interface continuity conditions.

4.3. Interface equation and Robin-Robin-GMRes algorithm.

Consider the Double-Loop algorithm. At each external iteration, we have to solve a fully-linearized FSI problem, in a given fluid geometry. The strategy considered in the previous section to solve this problem, can also be seen as a Richardson method applied to a preconditioned interface problem [3]. To illustrate this, first consider the linearized problem with Dirichlet-Neumann interface conditions (i.e. $\alpha_f \to \infty$ and $\alpha_s = 0$). After spatial discretization, e.g. by finite elements [38], this problem reads

$$\begin{bmatrix} C_{ff} & C_{f\Sigma} & 0 & 0 & 0 & 0 \\ 0 & M_\Sigma & 0 & 0 & -M_\Sigma & 0 \\ C_{\Sigma f} & C_{\Sigma\Sigma} & \widehat{M}_\Sigma & 0 & 0 & 0 \\ 0 & 0 & 0 & \widehat{M}_\Sigma & N_{\Sigma\Sigma} & N_{\Sigma s} \\ 0 & 0 & \widehat{M}_\Sigma & \widehat{M}_\Sigma & 0 & 0 \\ 0 & 0 & 0 & 0 & N_{s\Sigma} & N_{ss} \end{bmatrix} \begin{bmatrix} \mathbf{V}_f \\ \mathbf{V}_\Sigma \\ \mathbf{\Lambda}_f \\ \mathbf{\Lambda}_s \\ \mathbf{U}_\Sigma \\ \mathbf{U}_s \end{bmatrix} = \begin{bmatrix} \mathbf{b}_f \\ \mathbf{0} \\ \mathbf{b}_{f\Sigma} \\ \mathbf{b}_{s\Sigma} \\ \mathbf{0} \\ \mathbf{b}_s \end{bmatrix}, \tag{4.5}$$

where we have split the degrees of freedom associated to nodes interior to the fluid and structure domains from those associated to the FSI interface (denoted with the subscript Σ). Moreover, we have written the linearized structure problem in terms of velocities instead of displacements. The vector $\mathbf{V}_f$ contains interior velocity values and all the pressure values for the fluid, $\mathbf{U}_s$ contains interior velocity values for the structure problem, whereas $\mathbf{V}_\Sigma$ and $\mathbf{U}_\Sigma$ contain the interface velocity values for the fluid and for the structure, respectively, while $\mathbf{\Lambda}_f$ and $\mathbf{\Lambda}_s$ are the approximations of the Lagrange multipliers. Matrices C and N represent the algebraic counterpart of the linearized Oseen operator $\widehat{\nabla}_{v_f}\mathcal{F}$ and of the linearized structure operator $\nabla_{\eta_s}\mathcal{S}$, respectively. M_Σ is the interface mass matrix, which is invertible, so that the second equation is equivalent to the physical interface condition $\mathbf{V}_\Sigma = \mathbf{U}_\Sigma$. $\widehat{M}_\Sigma$ could be different from the interface mass matrix M_Σ, depending on the discretization used for the Lagrange multipliers. We assume here this matrix to be invertible. This is guaranteed, for instance, if one discretizes the Lagrange multipliers in the space of traces of velocity functions. The 5-th equation enforces the continuity of normal stresses at the FS interface. The right-hand sides follow accordingly to (3.4).

As suggested in [9, 32] the linearized FSI problem can also be understood as an interface problem in which the only unknown is the velocity at the fluid-structure interface. At the continuous level, the interface problem makes use of the fluid and structure Steklov-Poincaré operators (see e.g. [9]). Its fully discrete counterpart makes use of the fluid and structure Schur complement matrices (discrete versions of the Steklov-Poincaré operators, see [4]). System (4.5) is equivalent to

$$(\widetilde{C}_\Sigma + \widetilde{N}_\Sigma)\mathbf{U}_\Sigma = \widetilde{\mathbf{b}}_\Sigma \tag{4.6}$$

where

$$\widetilde{C}_\Sigma = C_{\Sigma\Sigma} - C_{\Sigma f} C_{ff}^{-1} C_{f\Sigma}, \tag{4.7a}$$

$$\widetilde{N}_\Sigma = N_{\Sigma\Sigma} - N_{\Sigma s} N_{ss}^{-1} N_{s\Sigma} \tag{4.7b}$$

are the fluid and structure Schur complement matrices and

$$\widetilde{\mathbf{b}}_\Sigma = \mathbf{b}_\Sigma - C_{\Sigma f} C_{ff}^{-1} \mathbf{b}_f - N_{\Sigma s} N_{ss}^{-1} \mathbf{b}_s$$

is the corresponding right-hand side.

It has been shown in [3] that the Robin-Robin partitioned procedure described in Algorithm 3, point 2, can be interpreted as a Richardson method over the preconditioned system (RR-Richardson)

$$\widetilde{P}_{RR}^{-1}(\widetilde{C}_\Sigma + \widetilde{N}_\Sigma)\mathbf{U}_\Sigma = \widetilde{P}_{RR}^{-1}\widetilde{\mathbf{b}}_\Sigma, \tag{4.8}$$

the preconditioner being

$$\widetilde{P}_{RR} = \frac{1}{\alpha_f + \alpha_s}\left(\widetilde{C}_\Sigma + \alpha_f M_\Sigma\right) M_\Sigma^{-1}\left(\widetilde{N}_\Sigma + \alpha_s M_\Sigma\right). \tag{4.9}$$

Instead of a Richardson method, it is then possible to apply more performing Krylov methods to (4.8)-(4.9), such as GMRes. In this way, we obtain again a partitioned procedure, composed of successive solutions of Dirichlet-structure problems, Robin-structure problems and Robin-fluid problems [3]. These procedures could be used alternatively to the RR-Richardson one at step 2 in Algorithm 3.

5. The added mass effect

In this section we recall the concept of added mass and its role in the stability of explicit (staggered) partitioned algorithms as well as in the convergence properties of fixed point type iterations for implicit partitioned algorithms.

We study a very simple problem of an inviscid incompressible fluid in a pipe pushed against an elastically supported rigid plate, with the eventual introduction of a dumper (piston problem). The dynamics of the plate is governed by a simple second order ordinary differential equation, whereas the dynamics of the fluid can be described as a potential flow. Figure 2 illustrates the set up of the problem. We also assume small displacements, so that the fluid domain is considered fixed, and small velocities, so that the fluid equations could be linearized around the rest state $\boldsymbol{u}_f = \mathbf{0}$. In particular, we have the following coupled problem

$$\begin{cases} \rho_f \dfrac{\partial \boldsymbol{u}_f}{\partial t} + \nabla p_f = \mathbf{0} & \text{in } \Omega_f, \\ \nabla \cdot \boldsymbol{u}_f = 0 & \text{in } \Omega_f, \\ \boldsymbol{u}_f \cdot \boldsymbol{n} = 0 & \text{on } \Gamma_{wall}, \\ p_f = g & \text{on } \Gamma_{in}, \\ \boldsymbol{u}_f \cdot \boldsymbol{n} = \dot{\eta}_s & \text{on } \Gamma_p, \\ m\ddot{\eta}_s + c\dot{\eta}_s + k\eta_s = \int_{\Gamma_p} p_f \, d\gamma & \text{on } \Gamma_p, \end{cases} \tag{5.1}$$

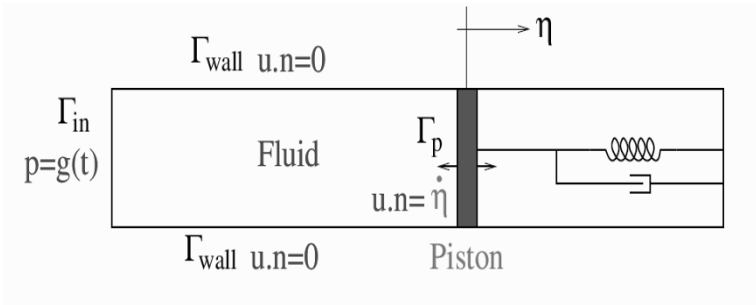

FIGURE 2. Schematic representation of the piston problem.

where g is a given datum and m, c, k are the mass, dumping and stiffness parameters representing the piston system. The last two conditions represent the continuity of the velocity and of the stress at the interface Γ_p.

By applying the divergence operator to the fluid momentum equation, it is possible to write an equivalent coupled problem involving just the fluid pressure and the piston displacement, as follows

$$\begin{cases} \triangle p_f = 0 & \text{in } \Omega_f, \\ \dfrac{\partial p_f}{\partial \boldsymbol{n}} = 0 & \text{on } \Gamma_{wall}, \\ p_f = g & \text{on } \Gamma_{in}, \\ \dfrac{\partial p_f}{\partial \boldsymbol{n}} = -\rho_f \ddot{\eta}_s & \text{on } \Gamma_p, \\ m\ddot{\eta}_s + c\dot{\eta}_s + k\eta_s = \int_{\Gamma_p} p_f \, d\gamma & \text{on } \Gamma_p, \end{cases}$$

where the velocity interface condition has been written in terms of normal derivative of the pressure, since from the momentum equation projected in the normal direction we have

$$\boldsymbol{n} \cdot \left(\rho_f \frac{\partial \boldsymbol{u}_f}{\partial t} + \nabla p_f \right) = 0 \quad \rightarrow \quad \frac{\partial p_f}{\partial \boldsymbol{n}} = -\rho_f \frac{\partial (\boldsymbol{u}_f \cdot \boldsymbol{n})}{\partial t} \quad \text{on } \Gamma_p \cup \Gamma_{wall}.$$

Given $\xi \in \mathbb{R}$, consider now the following problem in the unknown w

$$\begin{cases} \triangle w = 0 & \text{in } \Omega_f, \\ \dfrac{\partial w}{\partial \boldsymbol{n}} = 0 & \text{on } \Gamma_{wall}, \\ w = 0 & \text{on } \Gamma_{in}, \\ \dfrac{\partial w}{\partial \boldsymbol{n}} = \xi & \text{on } \Gamma_p. \end{cases}$$

We introduce the *added mass operator* $\mathcal{M}_A : \mathbb{R} \to \mathbb{R}$ defined as follows

$$\mathcal{M}_A \, \xi := \rho_f \int_{\Gamma_p} w \, d\gamma.$$

In the specific setting considered here, the operator $\mathcal{M}_A$ is just a positive number with the units of a mass. It is easy to show that, for this example, $\mathcal{M}_A = \rho_f |\Omega_f|$, and

coincides with the total mass of the fluid contained in the pipe. In the general case of a deformable structure, the added mass operator is nothing but the *Neumann-to-Dirichlet* map related to the interface Γ_p multiplied by the factor ρ_f (see [7] for a precise definition).

By exploiting the linearity of the fluid problem, we have that the force exerted by the fluid on the piston can be written as

$$\int_{\Gamma_p} p_f \, d\gamma = \int_{\Gamma_p} p_g \, d\gamma - \mathcal{M}_A \, \ddot{\eta}, \tag{5.2}$$

for a suitable function p_g which takes into account the non-homogeneous boundary conditions on Γ_{in} and does not depend on the coupling with the piston. Then, the *effective* piston dynamics reads

$$(m + \mathcal{M}_A)\ddot{\eta}_s + c\dot{\eta}_s + k\eta_s = \int_{\Gamma_p} p_g \, d\gamma \quad \text{on } \Gamma_p. \tag{5.3}$$

This modified equation highlights that the effective mass of the piston includes the mass $\mathcal{M}_A$ of the fluid that has to be displaced. We also observe that the presence of the fluid alters the natural frequency of oscillation of the piston, which decreases from $\omega = \sqrt{k/m}$ in air to $\omega = \sqrt{k/(m + \mathcal{M}_A)}$ in the fluid.

We now focus on a BDFp discretization of equation (5.1). To lighten the presentation, we omit to detail the boundary conditions on the fixed boundaries of the pipe (inflow and wall). The discretized problem reads:

$$\begin{cases} \rho_f \frac{D_p \boldsymbol{u}_f^{n+1}}{\Delta t} + \nabla p_f^{n+1} = \mathbf{0} & \text{in } \Omega_f, \\ \nabla \cdot \boldsymbol{u}_f^{n+1} = 0 & \text{in } \Omega_f, \\ \boldsymbol{u}_f^{n+1} \cdot \boldsymbol{n} = \frac{D_p \eta_s^{n+1}}{\Delta t} & \text{on } \Gamma_p, \\ m \frac{D_p^2 \eta_s^{n+1}}{\Delta t^2} + c \frac{D_p \eta_s^{n+1}}{\Delta t} + k\eta_s^{n+1} = \int_{\Gamma_p} p_f^{n+1} \, d\gamma & \text{on } \Gamma_p. \end{cases} \tag{5.4}$$

In the next sections we analyze several explicit and implicit partitioned procedures to solve numerically the coupled problem (5.4).

5.1. Staggered Dirichlet-Neumann scheme

The first strategy we consider consists in extrapolating the force on the piston $\int_{\Gamma_p} p_f^{n+1}$ in $(5.4)_4$ with a q-th ($q \geq 1$) order extrapolation formula that uses the q previous evaluations $(p_f^n, p_f^{n-1}, \ldots, p_f^{n-q+1})$, namely

$$E_q(p_f^{n+1}) = \sum_{i=1}^{q} (-1)^{i+1} \binom{q}{i} p_f^{n+1-i}.$$

The scheme reads:

$$
\begin{aligned}
& m\frac{D_p^2\eta_s^{n+1}}{\Delta t^2} + c\frac{D_p\eta_s^{n+1}}{\Delta t} + k\eta_s^{n+1} = E_q\left(\int_{\Gamma_p} p_f^{n+1}\, d\gamma\right) \qquad \text{on } \Gamma_p, \\
& \begin{cases} \rho_f \frac{D_p \boldsymbol{u}_f^{n+1}}{\Delta t} + \nabla p_f^{n+1} = \mathbf{0} & \text{in } \Omega_f, \\ \nabla \cdot \boldsymbol{u}_f^{n+1} = 0 & \text{in } \Omega_f, \\ \boldsymbol{u}_f^{n+1} \cdot \boldsymbol{n} = \frac{D_p \eta_s^{n+1}}{\Delta t} & \text{on } \Gamma_p. \end{cases}
\end{aligned} \tag{5.5}
$$

This strategy leads to a staggered Dirichlet-Neumann algorithm where, at each time step, we can first solve the piston equation, using previous evaluations of the fluid pressure ("Neumann datum"), and then solve the fluid equations once the piston displacement is know ("Dirichlet datum"). The following result generalizes to BDFp schemes the one given in [7].

Lemma 5.1. *Let* $\bar{\beta}_p = 2\sum_{i=0}^{\lfloor p/2 \rfloor} \beta_{2i+1}$ *and* $\bar{\xi}_p = 2\sum_{i=0}^{\lfloor (p+1)/2 \rfloor} \xi_{2i+1}$. *The staggered Dirichlet-Neumann algorithm* (5.5) *is* unstable *if*

$$
\mathcal{M}_A > \frac{1}{(2^q-1)\bar{\beta}_p^2}\left(m\bar{\xi}_p + \Delta t c\bar{\beta}_p + \Delta t^2 k\right). \tag{5.6}
$$

Proof. The pressure equation corresponding to (5.5) is

$$
\begin{cases} \triangle p_f^{n+1} = 0 & \text{in } \Omega_f, \\ \dfrac{\partial p_f^{n+1}}{\partial \boldsymbol{n}} = -\rho_f \dfrac{D_p D_p \eta_s^{n+1}}{\Delta t^2} & \text{on } \Gamma_p, \end{cases} \tag{5.7}
$$

so the equivalent discretized scheme for the *effective* piston dynamics reads:

$$
m\frac{D_p^2\eta_s^{n+1}}{\Delta t^2} + c\frac{D_p\eta_s^{n+1}}{\Delta t} + k\eta_s^{n+1} = -\frac{\mathcal{M}_A}{\Delta t^2} E_q\left(D_p D_p \eta_s^{n+1}\right) + E_q\left(\int_{\Gamma_p} p_g^{n+1}\, d\gamma\right). \tag{5.8}
$$

The latter is a difference equation of order $2p+q$ of the form

$$
\alpha_0\eta_s^{n+1} + \alpha_1\eta_s^n + \ldots + \alpha_{2p+q}\eta_s^{n-(2p+q-1)} = \sum_{j=1}^{q}(-1)^{j+1}\binom{q}{j}\int_{\Gamma_p} p_g^{n-j+1}, \tag{5.9}
$$

with $\alpha_0 = \frac{m\beta_0}{\Delta t^2} + \frac{c\xi_0}{\Delta t} + k > 0$. Let us denote by $r(s)$ its characteristic polynomial of degree $2p+q$ and evaluate it in $s=-1$. Observe that this corresponds to evaluating the left-hand side of (5.9) for the sequence $\bar{\eta}_s^k = (-1)^k$, $k = 0, 1, \ldots$, i.e. $r(-1) = \sum_{i=0}^{2p+q} \alpha_i \bar{\eta}_s^{2p+q-i}$. Recalling that by consistency of the BDFp formulae it holds $\beta_0 =$

$\sum_{i=1}^{p} \beta_i$ and $\xi_0 = \sum_{i=1}^{p+1} \xi_i$, we have:

$$D_p \bar{\eta}_s^k = \beta_0 \bar{\eta}_s^k - \sum_{i=1}^{p} \beta_i \bar{\eta}_s^{k-i} = (-1)^k \left(\beta_0 - \sum_{i=1}^{p} (-1)^i \beta_i \right) = \bar{\beta}_p \bar{\eta}_s^k,$$

$$E_q(\bar{\eta}_s^k) = \sum_{i=1}^{q} (-1)^{i+1} \binom{q}{i} \bar{\eta}_s^{k-i} = (-1)^{k+1} (2^q - 1) = -(2^q - 1) \bar{\eta}_s^k,$$

$$D_p^2 \bar{\eta}_s^k = \xi_0 \bar{\eta}_s^k - \sum_{i=1}^{p+1} \xi_i \bar{\eta}_s^{k-i} = (-1)^k \left(\xi_0 - \sum_{i=1}^{p+1} (-1)^i \xi_i \right) = \bar{\xi}_p \bar{\eta}_s^k.$$

Then, (5.8) with $p_g^n = 0$, $n = 0, 1, \ldots,$ becomes

$$\frac{m\bar{\xi}_p}{\Delta t^2} \bar{\eta}_s^{n+1} + \frac{c\bar{\beta}_p}{\Delta t} \bar{\eta}_s^{n+1} + k \bar{\eta}_s^{n+1} = \frac{\mathcal{M}_A (2^q - 1) \bar{\beta}_p^2}{\Delta t^2} \bar{\eta}_s^{n+1}$$

and

$$r(-1) = (-1)^{2p+q} \left[\frac{m\bar{\xi}_p - \mathcal{M}_A (2^q - 1) \bar{\beta}_p^2}{\Delta t^2} + \frac{c\bar{\beta}_p}{\Delta t} + k \right].$$

We therefore see that for q even, $r(-\infty) = +\infty$ and under condition (5.6) $r(-1) < 0$. Therefore the characteristic polynomial has a root $s^* < -1$ which shows that the scheme is unstable. An analogous argument holds for q odd. □

Remark 5.2. Observe that under the condition

$$\mathcal{M}_A > \frac{m\bar{\xi}_p}{(2^q - 1)\bar{\beta}_p^2}$$

even if the difference equation (5.8) might be stable for some Δt large enough, it becomes unstable in the limit $\Delta t \to 0$. Hence, the scheme is asymptotically unstable and therefore not convergent.

If we take $q = p$ in (5.8) the value of the added mass $\mathcal{M}_A$ beyond which the scheme is unstable becomes smaller and smaller as p increases. In particular, for $p = 1, \ldots, 4$ we have

	p=1	p=2	p=3	p=4
$\mathcal{M}_A/m >$	1	1/4	3/35	1/32

Remark 5.3. The intuitive reason why algorithm (5.5) fails to be stable for large added mass is that the presence of the fluid on the structure appears as an extra inertia term. Any staggered procedure will treat that inertia term explicitly in the effective structure equation. If the fluid inertia term turns out to be larger than the structure inertia term, the staggered scheme is unstable and there is no way to stabilize it by reducing the time step Δt as both inertia terms are multiplied by the same power of Δt.

5.2. Implicit scheme with Dirichlet-Neumann subiterations

If no extrapolation of the forcing term on the structure is performed, we have to solve the coupled problem (5.4). For this, we consider Dirichlet-Neumann subiterations. For a given quantity x, at time step $n+1$ let $\{x_k^{n+1}\}$ be the sequence $\{x^0, x^1, \ldots, x^n, x^{n+1,k}\}$ with x^i, $i = 0 \ldots, n$ known from previous time iterations and $x^{n+1,k}$ unknown, k denoting the subiteration counter. Then, the Dirichlet-Neumann subiterations with relaxation read: given $\eta_{s,0}^{n+1}$, compute for $k = 1, \ldots$

$$\begin{cases} \rho_f \frac{D_p \boldsymbol{u}_{f,k}^{n+1}}{\Delta t} + \nabla p_f^{n+1,k} = \mathbf{0} & \text{in } \Omega_f, \\ \nabla \cdot \boldsymbol{u}_f^{n+1,k} = 0 & \text{in } \Omega_f, \\ \boldsymbol{u}_f^{n+1,k} \cdot \boldsymbol{n} = \frac{D_p \eta_{s,k-1}^{n+1}}{\Delta t} & \text{on } \Gamma_p, \end{cases} \tag{5.10}$$

$$m\frac{D_p^2 \widetilde{\eta}_{s,k}^{n+1}}{\Delta t^2} + c\frac{D_p \widetilde{\eta}_{s,k}^{n+1}}{\Delta t} + k\widetilde{\eta}_s^{n+1,k} = \int_{\Gamma_p} p_f^{n+1,k}\, d\gamma \quad \text{on } \Gamma_p,$$

$$\eta_s^{n+1,k} = \omega \widetilde{\eta}_s^{n+1,k} + (1-\omega)\eta_s^{n+1,k-1}.$$

The convergence of this fixed point algorithm can be easily analyzed by looking at the equivalent fixed point algorithm on the effective piston equation, and characterized by means of the *asymptotic convergence factor* $\sigma(\omega)$ defined as the smallest positive number for which

$$|\eta_s^{n+1,k} - \eta_s^{n+1}| \leq \sigma(\omega)|\eta_s^{n+1,k-1} - \eta_s^{n+1}| \quad \forall k = 1, 2, \ldots,$$

where η_s^{n+1} is the solution of the coupled problem (5.4). The result is summarized in the following Lemma, which generalizes to BDFp discretizations the result in [2].

Lemma 5.4. *The algorithm* (5.5) *converges to the solution of* (5.4) *if the relaxation parameter satisfies*

$$\omega \leq \frac{2}{1 + \frac{\mathcal{M}_A \beta_0^2}{m\xi_0 + \Delta t c \beta_0 + \Delta t^2 k}}.$$

Moreover, the best choice of ω *leads to an asymptotic convergence factor*

$$\sigma(\omega_{opt}) = \frac{1}{1 + \frac{\mathcal{M}_A \beta_0^2}{m\xi_0 + \Delta t c \beta_0 + \Delta t^2 k}}.$$

We see from this lemma that if the added mass of the fluid is large, i.e. $\mathcal{M}_A \gg m\xi_0/\beta_0^2$, then a very strong relaxation is needed ($\omega \ll 1$) and even with optimal choice of the relaxation parameter, the convergence will be very slow.

5.3. Robin-Robin procedures and optimal choices of the Robin coefficients

We now turn to Robin-Robin algorithms, either explicit or implicit applied to the coupled problem (5.4). Recalling the formulae (3.3) for the BDFp approximation of

time derivatives, we can write:

$$\boldsymbol{u}_f^{n+1}\cdot\boldsymbol{n}=\frac{D_p\eta_s^{n+1}}{\Delta t}=\frac{\beta_0}{\Delta t}\eta_s^{n+1}-f_s^n, \tag{5.11}$$

$$\frac{D_p^2\eta_s^{n+1}}{\Delta t^2}=\frac{\xi_0}{\Delta t^2}\eta_s^{n+1}-g_s^n=\frac{\xi_0}{\Delta t\beta_0}\boldsymbol{u}_f^{n+1}\cdot\boldsymbol{n}+\frac{\xi_0}{\Delta t\beta_0}f_s^n-g_s^n, \tag{5.12}$$

with $f_s^n=\frac{1}{\Delta t}\sum_{i=1}^{p}\beta_i\eta^{n+1-i}$ and $g_s^n=\frac{1}{\Delta t^2}\sum_{i=1}^{p+1}\xi_i\eta^{n+1-i}$, known from previous time steps. Therefore, the coupled FSI problem (5.4) can be written in the only unknowns $\boldsymbol{u}_f^{n+1}$ and p_f^{n+1} as

$$\begin{cases}\rho_f\frac{D_p\boldsymbol{u}_f^{n+1}}{\Delta t}+\nabla p_f^{n+1}=\boldsymbol{0} & \text{in } \Omega_f,\\ \nabla\cdot\boldsymbol{u}_f^{n+1}=0 & \text{in } \Omega_f,\\ \left(\frac{m\xi_0}{\Delta t\beta_0}+c+\frac{k\Delta t}{\beta_0}\right)\boldsymbol{u}_f^{n+1}\cdot\boldsymbol{n}-\int_{\Gamma_p}p_f^{n+1}\,d\gamma=\widetilde{f}_s^n & \text{on } \Gamma_p,\\ \boldsymbol{u}_f^{n+1}\cdot\boldsymbol{n}=const & \text{on } \Gamma_p,\end{cases} \tag{5.13}$$

for a suitable right-hand side $\widetilde{f}_s^n$ and where with $(5.13)_4$ we have highlighted that in condition $(5.13)_3$ the term $\boldsymbol{u}_f^{n+1}\cdot\boldsymbol{n}$ has to be constant over Γ_p. Once this fluid problem has been solved, the structure displacement is recovered thanks to $(5.11)_1$, that is $\eta_s^{n+1}=\frac{\Delta t}{\beta_0}(\boldsymbol{u}_f^{n+1}\cdot\boldsymbol{n}+f_s^n)$. Equation $(5.13)_{3-4}$ can be seen as a *defective* Robin boundary condition and could be treated as suggested in [41, 34, 15].

This derivation shows that the coupled FSI piston problem (5.4) can be reinterpreted as just a fluid problem with a (defective) Robin boundary condition. Therefore, the use of Robin boundary conditions allows us to incorporate the structure equation as a boundary condition for the fluid and solve exactly the coupled problem without the need of extrapolating any term. Equivalently, an iterative procedure as (5.10) that uses the Robin boundary condition $(5.13)_{3-4}$ instead of a Dirichlet one, will converge in just one iteration.

This nice behavior is actually possible thanks to the very simple nature of the structure problem. For more complex structural models, it will not be possible to reduce exactly the FSI problem to just a fluid problem with a Robin boundary condition. However, the argument used to derive (5.13) suggests that a good Robin boundary condition for the fluid is given by

$$\alpha_f\widetilde{\gamma}_f\boldsymbol{v}_f+\widetilde{\boldsymbol{\lambda}}_f=\alpha_f\widetilde{\gamma}_s\frac{D_p\widetilde{\boldsymbol{\eta}}_s}{\Delta t}-\widetilde{\boldsymbol{\lambda}}_s\quad\text{on }\Sigma^0, \tag{5.14}$$

with

$$\alpha_f\approx\frac{m\xi_0}{\Delta t\beta_0}+c+\frac{k\Delta t}{\beta_0}, \tag{5.15}$$

m, c, k being indicative mass, damping and elastic coefficients per unit area of the structure. In the case of a thin linear elastic structure with membrane deformation a quantitative formula for α_f has been proposed in [2, 34]. Then, an iterative procedure at each time step can be set up, in which the fluid subproblem is solved with suitable Robin boundary conditions whereas the structure problem is solved with Neumann boundary conditions. We name this strategy Robin-Neumann (RN) algorithm.

The good convergence property of the RN scheme with (5.15) for FSI problems has been confirmed by the analysis provided in [2], which highlights that for a model problem as the one presented in (5.1), but with a one-dimensional elastic structure described by the generalized string model, convergence is achieved without any relaxation ($\omega = 1$) and with asymptotic convergence factor $\sigma(1) \ll 1$ very insensitive to the ratio ρ_f/ρ_s (i.e. to the added mass effect).

It is now possible to ask whether a Robin interface condition also for the structure side could improve the convergence properties (Robin-Robin scheme). Turning then our attention to Robin boundary conditions for the structure problem and the choice of the parameter α_s, a way to partially include the fluid model as a boundary condition for the structure is provided by equation (5.2). Indeed, from this relation and assuming negligible the viscous fluid forces in the normal direction with respect to the pressure, we obtain

$$\begin{aligned}\boldsymbol{T}_s^{n+1}\boldsymbol{n}_s \cdot \boldsymbol{n}_s = -\boldsymbol{T}_f^{n+1}\boldsymbol{n}_f \cdot \boldsymbol{n}_s &\simeq -p_f^{n+1} \\ &\simeq \mathcal{M}_A \frac{D_p D_p}{\Delta t^2}\eta_s^{n+1} - p_g = \mathcal{M}_A \frac{\beta_0^2}{\Delta t}\eta_s^{n+1} - \mathcal{M}_A g_s^n - p_g,\end{aligned}$$

which leads to the heuristic value $\alpha_s = \frac{\beta_0^2}{\Delta t}\mathcal{M}_A$.

However, this choice is not directly usable for complex FSI problems, since $\mathcal{M}_A$ is, in general, an operator and not just a number as in the piston model problem. For this reason, a different strategy based on the minimization of a reduction factor has been considered in [19]. In particular, in this work the authors considered a two-dimensional coupled Stokes - Incompressible Linear Elasticity problem defined in the whole plane and used Fourier analysis to derive an optimized coefficient, in the spirit of the Optimized Schwartz Methods [18]. The optimization leads to the following value

$$\alpha_s = \frac{2}{\Delta t\, k^*}\sqrt{\rho_f + \mu\Delta t\,(k^*)^2}\left(\sqrt{\mu\Delta t}\,k^* + \sqrt{\rho_f + \mu\Delta t\,(k^*)^2}\right), \tag{5.16}$$

with $k^* = \sqrt{\frac{\beta_0\rho_f(\sqrt{5}-1)}{2\mu\Delta t}}$.

6. Summary of the performances in numerical experiments

In this section, we review the performance featured by the partitioned procedures presented in this work in numerical experiments developed in some recent works [9, 4, 2, 3, 19, 34, 35].

The naive approach presented in Algorithm 1 has shown to be slower than the quasi-Newton methods of about 3 times [35]. However, it has shown to be the easiest to implement in a modular way. The test case considered in [35] is a realistic 3D carotid bifurcation reconstructed from MRI images, with physiological data.

The Dirichlet-Neumann Richardson procedure has been usually implemented with an Aitken procedure to estimate *in itinere* an optimal value for the relaxation

parameter ω (see e.g. [9, 29]). Experience shows that with this strategy the convergence is always achieved both in 2D and in 3D applications. In typical haemodynamic applications, where the density of the fluid and the structure are comparable and the added mass of the fluid on the structure is large, the convergence is however relatively slow even with the Aitken extrapolation procedure, as reported in [2, 9].

The DN-GMRes procedure introduced in [4] features a weaker sensitivity to the added mass effect than DN-Richardson iterations, and convergence is achieved without any relaxation also in test cases on real geometries. It has been reported in [4, Figure 1], on a 2D test case, that the DN-GMRes requires a number of iterations smaller by approximately a factor 10 than DN-Richardson with an optimally chosen fixed relaxation parameter.

Concerning the RN-Richardson procedure, 2D numerical results have been presented in [2], where it has been highlighted that convergence is always achieved without any relaxation, independently of the ratio between the fluid and structure densities. This performance has also been confirmed in real 3D applications with linear elastic models in [34] and non linear finite elasticity in [35]. The numerical results in [2] show an improvement of at least a factor two between RN-Richardson (without any relaxation) and DN-Richardson with Aitken acceleration. No substantial improvement has been observed, instead, by using the Aitken procedure for RN-Richardson.

As for the RR-Richardson method, in [19] it has been shown that in 2D cases the use of (5.16) improves the numerical performance of about 50% with respect to RN-Richardson ($\alpha_s = 0$). This procedure with such a value of α_s has shown better convergence properties also in 3D real cases [34].

The numerical results presented in [3] showed that the convergence of the RR-GMRes strategy seems to be much less sensitive to the choice of the Robin parameters α_f and α_s, than the corresponding RR-Richardson iterations, where such parameters have to be properly tuned to obtain fast convergence. This is a nice feature when real geometries are considered, since the optimal value of α_f for RR-Richardson should take into account the curvature of the vessel, while with RR-GMRes a constant value obtained by considering average quantities is enough to achieve good convergence properties. On the other hand, RR-GMRes has a slightly higher computational cost per iteration with respect to RR-Richardson as it requires 2 structural problems + 1 fluid problem (or equivalently 2 fluid problems + 1 structure problem) per iteration compared to the 1 structure + 1 fluid problem of the RR-Richardson method.

Another nice feature of RR procedures is that they allow to solve without any complication an enclosed fluid problem, that is a FSI problem where Dirichlet or flow rate boundary conditions are enforced on all portions of the fluid domain except the FS interface. Indeed, in this case, DN procedures fail to produce an accurate solution, since the conservation of mass is not guaranteed at each iteration. Specific treatment, such as Lagrange multipliers, have to be considered to solve such problems. On the contrary, with RR procedures this kind of problems could be solved without any modification of the standard partitioned algorithms [3].

References

[1] M. Astorino, F. Chouly, and M. Fernández. Robin based semi-implicit coupling in fluid-structure interaction: stability analysis and numerics. *SIAM J. Sci. Comp.*, 31(6):4041–4065, 2009.

[2] S. Badia, F. Nobile, and C. Vergara. Fluid-structure partitioned procedures based on Robin transmission conditions. *J. Comput. Physics*, 227:7027–7051, 2008.

[3] S. Badia, F. Nobile, and C. Vergara. Robin-Robin preconditioned Krylov methods for fluid-structure interaction problems. *Comput. Methods Appl. Mech. Engrg.*, 198(33-36):2768–2784, 2009.

[4] S. Badia, A. Quaini, and A. Quarteroni. Modular vs. non-modular preconditioners for fluid-structure systems with large added-mass effect. *Comput. Methods Appl. Mech. Engrg.*, 197:4216–4232, 2008.

[5] S. Badia, A. Quaini, and A. Quarteroni. Splitting methods based on algebraic factorization for fluid-structure interaction. *SIAM J. Sci. Comp.*, 30(4):1778–1805, 2008.

[6] Y. Bazilevs, V.M. Calo, Y. Zhang, and T.J.R. Hughes. Isogeometric fluid-structure interaction analysis with applications to arterial blood flow. *Computational Mechanics*, 38:310–322, 2006.

[7] P. Causin, J.F. Gerbeau, and F. Nobile. Added-mass effect in the design of partitioned algorithms for fluid-structure problems. *Comput. Methods Appl. Mech. Engrg.*, 194(42-44):4506–4527, 2005.

[8] J. Degroote. Artificial added mass instabilities in sequential staggered coupling of nonlinear structures and incompressible viscous flow. *J. Comput. Physics*, 230(17):6399–6403, 2011.

[9] S. Deparis, M. Discacciati, G. Fourestey, and A. Quarteroni. Fluid-structure algorithms based on Steklov-Poincaré operators. *Comput. Methods Appl. Mech. Engrg.*, 195(41-43):5797–5812, 2006.

[10] W.G. Dettmer and D. Perić. On the coupling between fluid flow and mesh motion in the modelling of fluidstructure interaction. *Comp. Mech.*, 43:81–90, 2008.

[11] J. Donea. An arbitrary Lagrangian-Eulerian finite element method for transient dynamic fluid-structure interaction. *Comput. Methods Appl. Mech. Engrg.*, 33:689–723, 1982.

[12] M.A. Fernández, J.F. Gerbeau, and C. Grandmont. A projection semi-implicit scheme for the coupling of an elastic structure with an incompressible fluid. *Int. J. Num. Methods Engrg.*, 69(4):794–821, 2007.

[13] C. Figueroa, I. Vignon-Clementel, K. Jansen, T. Hughes, and C. Taylor. A coupled momentum method for modeling blood flow in three-dimensional deformable arteries. *Comput. Methods Appl. Mech. Engrg.*, 195:5685–5706, 2006.

[14] L. Formaggia, A. Quarteroni, and A. Veneziani (Eds.). *Cardiovascular Mathematics - Modeling and simulation of the circulatory system*. Springer, 2009.

[15] L. Formaggia and C. Vergara. Prescription of general defective boundary conditions in fluid-dynamics. *Milan Journal of Mathematics*, 2012. DOI:10.1007/s00032-012-0185-8.

[16] C. Forster, W. Wall, and E. Ramm. Artificial added mass instabilities in sequential staggered coupling of nonlinear structures and incompressible viscous flow. *Comput. Methods Appl. Mech. Engrg.*, 196(7):1278–1293, 2007.

[17] Y.C. Fung. *Biomechanics. Mechanical Properties of Living Tissues*. Springer, 2nd edition, 1993.

[18] M.J. Gander. Optimized Schwarz methods. *SIAM J. Numer. Anal.*, 44(2):699–731, 2006.

[19] L. Gerardo Giorda, F. Nobile, and C. Vergara. Analysis and optimization of Robin-Robin partitioned procedures in fluid-structure interaction problems. *SIAM J. Numer. Anal.*, 48(6):2091–2116, 2010.

[20] E. Hairer, S.P. Nørsett, and G. Wanner. *Solving ordinary differential equations: Nonstiff problems*. Springer Series in Comput. Math. Springer, 1993.

[21] M. Heil. An efficient solver for the fully coupled solution of large-displacement fluid-structure interaction problems. *Comput. Methods Appl. Mech. Engrg.*, 193:1–23, 2004.

[22] M. Heil, A. Hazel, and J. Boyle. Solvers for large-displacement fluidstructure interaction problems: segregated versus monolithic approaches. *Comp. Mech.*, 43(1):91–101, 2008.

[23] G.A. Holzapfel, T.C. Gasser, and R.W. Ogden. A new constitutive framework for arterial wall mechanics and a comparative study of material models. *J. Elasticity*, 61:1–48, 2000.

[24] G.A. Holzapfel and R.W. Ogden. Constitutive modelling of arteries. *Proc. R. Soc. Lond. Ser. A Math. Phys. Eng. Sci.*, 466(2118):1551–1596, 2010.

[25] T. J. R. Hughes, W. K. Liu, and T. K. Zimmermann. Lagrangian-Eulerian finite element formulation for incompressible viscous flows. *Comput. Methods Appl. Mech. Engrg.*, 29(3):329–349, 1981.

[26] C. Kassiotis, A. Ibrahimbegovic, R. Niekamp, and H. Matthies. Nonlinear fluid-structure interaction problem. part i: implicit partitioned algorithm, nonlinear stability proof and validation examples. *Comput. Mech.*, 47:305–323, 2011.

[27] R.M. Kirby, Z. Yosibash, and G.E. Karniadakis. Towards stable coupling methods for high-order discretization of fluid-structure interaction: Algorithms and observations. *J. Comput. Physics*, 223:489–518, 2007.

[28] U. Kuttler, M. Gee, Ch Forster, A Comerford, and W.A. Wall. Coupling strategies for biomedical fluid-structure interaction problems. *Int. J. Num. Methods Biomed. Engrg.*, 26:305–321, 2010.

[29] U. Kuttler and W.A. Wall. Fixed-point fluid-structure interaction solvers with dynamic relaxation. *Comput. Mech.*, 43:61–72, 2008.

[30] Y. Liu, C. Charles, M. Gracia, H. Gregersen, and G. S. Kassab. Surrounding tissues affect the passive mechanics of the vessel wall: theory and experiment. *Am. J. Physiol. Heart Circ. Physiol.*, 293:H3290–H3300, 2007.

[31] H.G. Matthies, R. Niekamp, and J. Steindorf. Algorithms for strong coupling procedures. *Computers & Structures*, 195:2028–2049, 2006.

[32] C. Michler, E. H. van Brummelen, and R. de Borst. An interface Newton-Krylov solver for fluid-structure interaction. *Int. J. Num. Methods Fluids*, 47(10-11):1189–1195, 2005.

[33] P. Moireau, N. Xiao, M. Astorino, C. A. Figueroa, D. Chapelle, C. A. Taylor, and J.-F. Gerbeau. External tissue support and fluidstructure simulation in blood flows. *Biomechanics and Modeling in Mechanobiology*, 11(1-2):1–18, 2012.

[34] F. Nobile, M. Pozzoli, and C. Vergara. Time accurate partitioned algorithms for the solution of fluid-structure interaction problems in haemodynamics. MOX-Report 30-2011, Department of Mathematics, Politecnico di Milano, Italy, 2011.

[35] F. Nobile, M. Pozzoli, and C. Vergara. Exact and inexact partitioned algorithms for fluid-structure interaction problems with finite elasticity in haemodynamics. MOX-Report 37-2012, Department of Mathematics, Politecnico di Milano, Italy, 2012.

[36] K. Perktold, E. Thurner, and T. Kenner. Flow and stress characteristics in rigid walled and compliant carotid artery bifurcation models. *Medical and Biological Engineering and Computing*, 32(1):19–26, 1994.

[37] S. Piperno and C. Farhat. Design of efficient partitioned procedures for transient solution of aerolastic problems. *Rev. Eur. Elements Finis*, 9(6-7):655–680, 2000.

[38] A. Quarteroni and A. Valli. *Numerical approximation of partial differential equations.* Springer, 1994.

[39] T.E. Tezduyar, S. Sathe, T. Cragin, B. Nanna, B.S. Conklin, J. Pausewang, and M. Schwaab. Modelling of fluid-structure interactions with the space-time finite elements: arterial fluid mechanics. *Int. J. Num. Methods Fluids*, 54:901–922, 2007.

[40] T.E. Tezduyar, S. Sathe, and K. Stein. Solution techniques for the fully discretized equations in computation of fluidstructure interactions with the spacetime formulations. *Comput. Methods Appl. Mech. Engrg.*, 195(41-43):57435753, 2006.

[41] C. Vergara. Nitsche's method for defective boundary value problems in incompressibile fluid-dynamics. *J. Sci. Comp.*, 46(1):100–123, 2011.

[42] R. Wulandana and A.M. Robertson. An inelastic multi-mechanism constitutive equation for cerebral arterial tissue. *Biomechanics and Modeling in Mechanobiology*, 4(4):235–248, 2005.

[43] H. Yang. Partitioned solvers for the fluid-structure interaction problems with a nearly incompressible elasticity model. *Comput. Visual. Sci.*, pages 243–267, 2012.

Fabio Nobile
MOX, Dipartimento di Matematica, Politecnico di Milano
Piazza Leonardo da Vinci 32
20133 Milano
Italy
and
CSQI – MATHICSE, École Polytechnique Fédérale de Lausanne
Station 8
1015 Lausanne
Switzerland
e-mail: fabio.nobile@epfl.ch

Christian Vergara
Dipartimento di Ingegneria dell'Informazione e Metodi Matematici, Università di Bergamo
Viale Marconi 5
24044 Dalmine (BG)
Italy
e-mail: christian.vergara@unibg.it

Received: May 2, 2012.